Nuclear Instruments and Methods in Physics Research A 768 (2014) 32–42

Contents lists available at ScienceDirect

Nuclear Instruments and Methods in Physics Research A

journal homepage: www.elsevier.com/locate/nima

Electro-optical characterization of MPPC detectors for the ASTRI Cherenkov telescope camera

D. Marano [a,*], M. Belluso [a], G. Bonanno [a], S. Billotta [a], A. Grillo [a], S. Garozzo [a], G. Romeo [a], O. Catalano [b], G. La Rosa [b], G. Sottile [b], D. Impiombato [b], S. Giarrusso [b]

[a] INAF, Osservatorio Astrofisico di Catania, Via S. Sofia 78, I-95123 Catania, Italy
[b] INAF, Istituto di Astrofisica Spaziale e Fisica Cosmica di Palermo, Via U. La Malfa 153, I-90146 Palermo, Italy

ARTICLE INFO

Article history:
Received 6 March 2014
Received in revised form
2 September 2014
Accepted 7 September 2014
Available online 18 September 2014

Keywords:
Detector performance
Electro-optical characterization
Photon detection efficiency
Silicon photomultipliers

ABSTRACT

This work addresses a systematic and in-depth electro-optical characterization of the Multi-Pixel Photon Counter (MPPC) sensors constituting the camera detection system at the focal plane of the ASTRI telescope prototype. The paper reports the experimental results of a large set of measurements on the MPPC devices in order to provide a reliable qualification of the detector performance and evaluate its compliance with the telescope focal plane requirements. In particular, breakdown voltage, internal gain, dark count rate, cross-talk and extra-charge probability, and absolute photon detection efficiency measurements are performed on the basic sensor device unit as a function of the detector operating conditions.

1. Introduction

The upcoming Cherenkov Telescope Array (CTA) is a worldwide project focused on the design, realization and operation of an array of approximately one hundred ground based new generation gamma-ray telescopes covering a wide energy range with a sensitivity in the core energy region (around 1 TeV) of nearly one order of magnitude greater than currently operating telescope arrays. Due to the different characteristics of the Cherenkov light signals within different energy bands, three kinds of telescope configurations will be implemented in order to provide the widest coverage of the energy spectrum: the low energy band (from 20 GeV up to 1 TeV) will be covered by large-size telescopes (LSTs) with 23-m diameter mirrors; the medium energy region (from 200 GeV up to 10 TeV) will be observed by medium-size telescopes (MSTs) with 9–12-m diameter primary mirrors; the highest energy band (from few TeV to 100 TeV) will be detected by small-size telescopes (SSTs) with 4–7- m diameter mirrors [1]. Two arrays will be deployed, one in the northern and the other one in the southern hemisphere, in order to provide all-sky coverage.

Astrofisica con Specchi a Tecnologia Replicante Italiana (ASTRI) is a flagship project currently being financed by the Italian Ministry of Education, University and Research (MIUR) and pursued by the Italian National Institute for Astrophysics (INAF), whose primary target is the development of an end-to-end Italian prototype of the SST devoted to the CTA survey of the highest gamma-ray energy range. This telescope, henceforth referred to as ASTRI SST-2M, is characterized by innovative technological solutions in terms of mirror structure, focal plane sensors and front-end electronics. It is foreseen to be installed, commissioned and fully operated under field conditions by the end of 2014 at the INAF "M.G. Fracastoro" observing station (1735 m a.s.l.) located in Serra La Nave, at the foot of Mount Etna (Catania, Sicily).

The ASTRI SST-2M prototype will be equipped with a wide field dual-mirror (2M) Schwarzschild–Couder (SC) optical system arranged in a compact layout configuration, empowering good angular resolution across the entire field of view (almost 10° in diameter) and reducing the effective focal length and camera dimensions. The optical approach adopted allows the exploitation of a compact, low-cost, light-weight and low-power consumption camera to be placed at the curved focal surface of the telescope [2].

Silicon Photo-Multipliers (SiPMs) are the semiconductor photosensor devices intended to equip the camera at the focal plane of the ASTRI SST-2M telescope. SiPM detectors operate at a relatively low bias voltage and feature high multiplication ratio, high photon detection efficiency, fast transient response, excellent time resolution and wide spectral response range; therefore, they are particularly suitable for photon counting applications and have a strong inherent potential for replacing traditional phototube detectors. Since the last few years, SiPM technology has been developing very quickly.

* Corresponding author.
E-mail address: davide.marano@oact.inaf.it (D. Marano).

http://dx.doi.org/10.1016/j.nima.2014.09.015
0168-9002/

New SiPM detectors with outstanding characteristics have been recently produced by the world leading manufacturers and further performance improvements are foreseen at short terms. Contextually, remarkable research activities have been worldwide undertaken by a rising number of companies and institutions [3–23].

SiPM photosensors are suitable for the detection of the Cherenkov flashes, since they are very fast and sensitive to the light in the 350–700 nm wavelength range. Their drawbacks compared to the traditional photo-multiplier tubes are high dark count rates, spurious after-pulsing, optical cross-talk contributions, and intrinsic gain factors strongly dependent on chip temperature. Nonetheless, the SiPM dark count rate is well below the night sky background (NSB) level, so that the instrumental background does not degrade the telescope sensitivity; in addition, the effects of cross-talk and afterpulses are typically restrained, and the gain can be kept stable against temperature variations by means of an adequate bias voltage compensation strategy.

The construction, commissioning and first observational campaigns of the ASTRI SST-2M prototype will allow an accurate testing of all telescope components (mechanics, mirrors, camera and front-end electronics) in real observing conditions, in order to confirm the effectiveness of the technological solutions adopted and verify the telescope's expected performance. Although the SST-2M telescope will mainly act as a technological prototype, it should be able to perform scientific observations as well. The ASTRI collaboration proposed the installation of a small array consisting of 5–7 SSTs at the selected CTA southern site. This small array could constitute the first CTA seed and will be used for technical purposes and scientific studies, mainly in the highest energy region from few to tens of TeV. This energy region is still widely unexplored and may lead to new unexpected discoveries.

This document presents and discusses the experimental results from a large set of measurements performed on the SiPM sensors to be used for the ASTRI SST-2M telescope camera, and is mainly aimed at characterizing the detector performance and confirming its compliance with the telescope focal plane requirements.

2. The ASTRI SST-2M telescope camera

The ASTRI SST-2M camera has truncated-cone shape with overall dimensions of about 50 cm × 50 cm × 50 cm, including mechanics and interfaces with the telescope structure, for a global weight of around 50 kg. Such detection surface requires a spatial segmentation of a few square millimeters to be compliant with the imaging resolving angular size (0.17°). Furthermore, the light sensor should offer a high photon detection sensitivity in the wavelength range between 300 nm and 700 nm and a fast temporal response.

Since the working energy range of the ASTRI SST-2M telescope is 1–100 TeV, the maximum number of photoelectrons detected in a single pixel, also according to the optics area, is estimated to be 1000, which is collected in a very short time duration (few nanoseconds).

In order to match the angular resolution of the optical system, the design of the ASTRI camera has to comply with the general idea of modularity. In other words, particular care has been devoted to the choice of dimensions for the basic detection module. Since the convex-shaped focal surface of the SST-2M camera has a curvature radius of about 1 m, the curved surface of the camera has to be fit with a certain number of square modules without losing the required focusing capability of the optical system. This specification is physically accomplished by a square module of about 6.2 × 6.2 mm^2, resulting in a sky-projected angular size of 0.17°.

Among the available SiPM sensors, the Hamamatsu S11828-3344 Multi-Pixel Photon Counter (MPPC) device has been selected for the ASTRI SST-2M prototype. The basic detector unit provided by the manufacturer is a monolithic multi-pixel MPPC consisting of a 4 × 4 matrix of squared pixels, each of which is nearly 3 × 3 mm^2 wide and made up of 3600 elementary photodiode microcells (SPADs) of 50-μm pitch with a 62% geometrical fill factor. Four SiPM pixels are physically grouped together into a unique logical macro-pixel with an overall physical size of 6.2 mm × 6.2 mm, corresponding to the required 0.17° optical angular resolution. The physical aggregation of 4 × 4 flat sensor units (8 × 8 logical pixels) forms the basic Photon Detection Module (PDM), composed of 16 MPPC monolithic devices with overall 56 × 56 mm^2 dimensions, and 37 structural PDMs are combined together at the focal plane of the telescope camera, delivering the required full optical field of view. To prevent accidental sunlight exposure of the focal surface detectors, the ASTRI SST-2M camera is equipped with a light-tight two-petal lid mounted onto the backbone structure of the camera. Fig. 1 depicts an overview of the camera box, on top of which 37 PDM modules are visible [20].

The way the detectors are assembled in a PDM module is illustrated in Fig. 2, showing a pictorial schematization of the baseline focal surface arrangement. Each SiPM unit consists of 4 logical channels, so that a complete PDM module will be constituted by 64 logical macro-pixels. In total, 37 structural modules are required to convey the information represented by the photoelectron pulse signals coming from the focal surface camera detectors. The single macro-pixel constituting the basic logical channel is highlighted in the picture by the yellow square box.

The main advantage of the ASTRI SST-2M camera design is that all basic PDMs are physically independent of each other, ensuring flexibility in maintenance and inspection of reduced portions of the camera, thus facilitating the replacement of faulty PDMs in any position of the focal surface camera. Furthermore, in consideration of the rapidly developing progress and innovation of SiPM fabrication technology, the mechanical structure and front-end electronics of the telescope camera are specifically designed such that the focal plane detectors of each single PDM can be easily interchangeable, allowing exploitation of different SiPM sensors of the same logical pixel dimensions.

3. Electronics of the ASTRI SST-2M camera

The ASTRI SST-2M camera electronics is designed to meet all the specifications required to catch the fast pulses produced by the MPPC detectors of the focal plane, to generate a trigger, manage signals, acquire and store the events data, and communicate to an external camera controller and to an external science console. According to the structural layout of the telescope, the electronics of the focal surface exhibits electrical and mechanical modularity at the PDM level. Moreover, each PDM works independently of the others, making it possible to replicate the electronics with clear benefits regarding debugging, harness complexity and manufacturing costs. The ASTRI SST-2M electronics assembly includes the

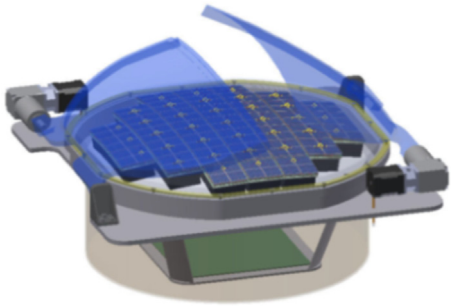

Fig. 1. Schematic of the ASTRI SST-2M telescope camera, with the 37 structural PDMs at the focal plane.

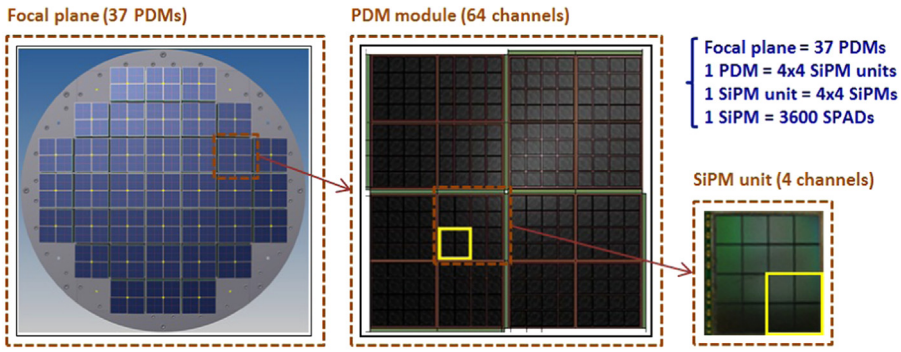

Fig. 2. Structural composition of the PDM modules on the ASTRI SST-2M telescope focal plane. (For interpretation of the references to color in this figure, the reader is referred to the web version of this article.)

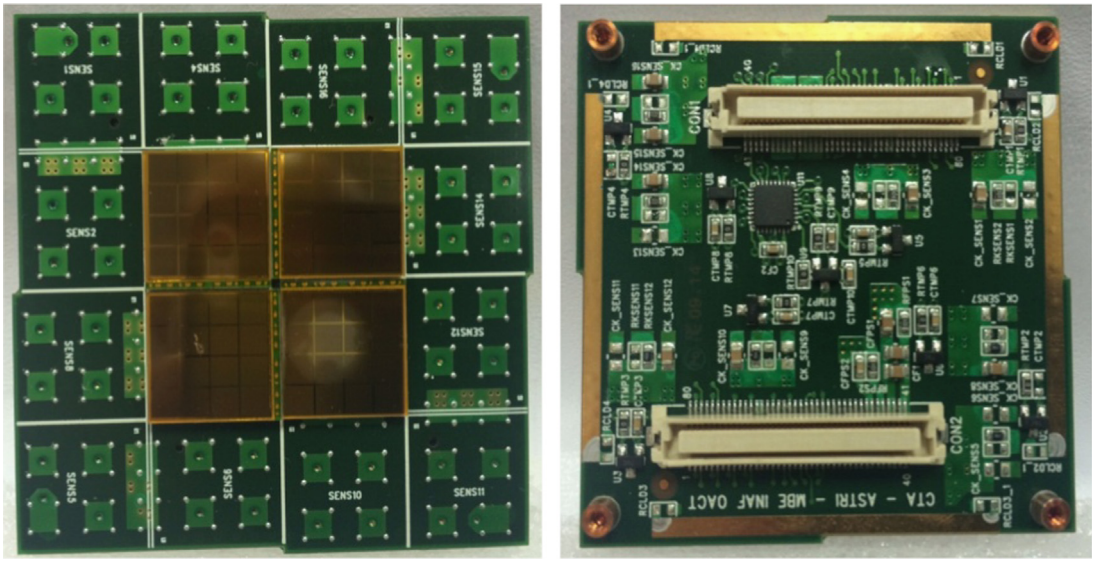

Fig. 3. PDM MPPC interface board top layer (on the left side) and bottom layer (on the right side).

focal plane electronics constituted by the MPPCs, the Front-End Electronics (FEE) and the Back-End Electronics (BEE).

The ASTRI telescope focal surface is composed of 37 PDM tiles, each one hosting the 16 monolithic MPPCs with associated FEE. The function of each FEE is to process and convert the analog SiPM signals into digital counts by exploiting 2 Application Specific Integrated Circuits (ASICs) interfacing the MPPC detectors, 4 Analog-to-Digital Converters (ADCs) and a Field Programmable Gate Array (FPGA) managing the ASICs slow control, local triggers generation and data acquisition. Each FPGA is also in charge of performing specific trigger algorithms.

The BEE is hosted on a separate common board and is based on a powerful Xilinx Zynq-7000 FPGA, integrating a feature-rich dual-core processor, which controls and manages the overall system including data management, lid mechanisms and optical fiber calibration tools. It additionally provides all functions necessary to process and transmit the event data obtained by each FEE.

The printed circuit board (PCB) realized to interface the MPPC detectors of each single PDM to the relevant FEE is illustrated in Fig. 3. Each monolithic MPPC device is soldered to the front side of the PCB exploiting a ball grid array soldering technique, ensuring an accurate placement of the SiPM detectors on the board. The MPPC detectors are assembled so as to conform with the mechanical structure of the board. The rear side of the board hosts two multi-pin connectors interfacing with the FEE, along with 8 RC filters for the MPPC voltage supply and 9 temperature sensors for thermal monitoring and gain stabilization.

The most critical part of the PDM electronics is the analog FEE, which must preserve the information contained in the signal pulses for further processing and measurements (i.e., energy and pixel time tagging). The very short duration of the Cherenkov light flashes associated to gamma-ray events requires a dedicated FEE capable of catching the very fast pulses of Cherenkov light and providing auto-trigger capability and fast camera pixel read-out.

The main element of the ASTRI SST-2M camera FEE is the "Cherenkov Image Telescope Integrated Read-Out Chip" (CITIROC) [4], which is an upgraded version of the "Extended Analogue SiPM Integrated Read-Out Chip" (EASIROC) [5], both produced by Omega. It is a 32-channel fully-analog front-end ASIC specifically designed to directly interface SiPM detectors, working as a signal shaper in which the amplitude of the analog peaks contains the value of the input signal integrated in a specific time window. Such operation is different with respect to other ASIC-based Cherenkov telescopes, sampling the input signal at typical rates of about 1 GHz; in fact, by this means, the data throughput in the ASTRI camera is sensibly reduced, as the event data are condensed in a single value.

The architecture of the CITIROC analog core is sketched in Fig. 4.

Each channel feeds a double chain of voltage-sensitive AC-coupled tunable-gain low-noise pre-amplifiers, one for high-gain (HG) and one for low-gain (LG) operation, in order to measure charge values from 160 fC up to 320 pC, corresponding to a range of 1–2000 photoelectrons (assuming an MPPC gain of 10^6) with a photoelectron-to-noise

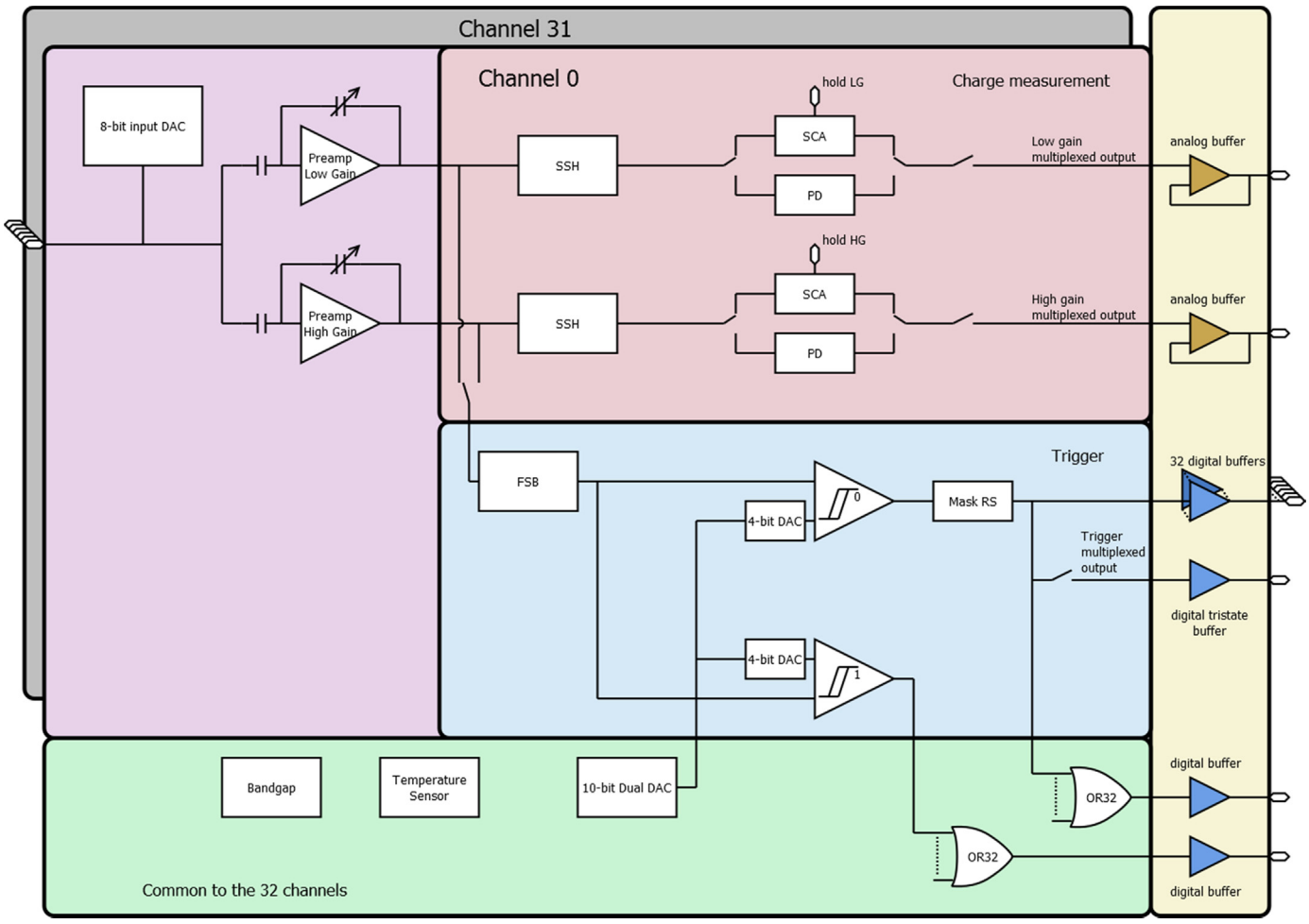

Fig. 4. Simplified block diagram of the CITIROC front-end (courtesy of Omega).

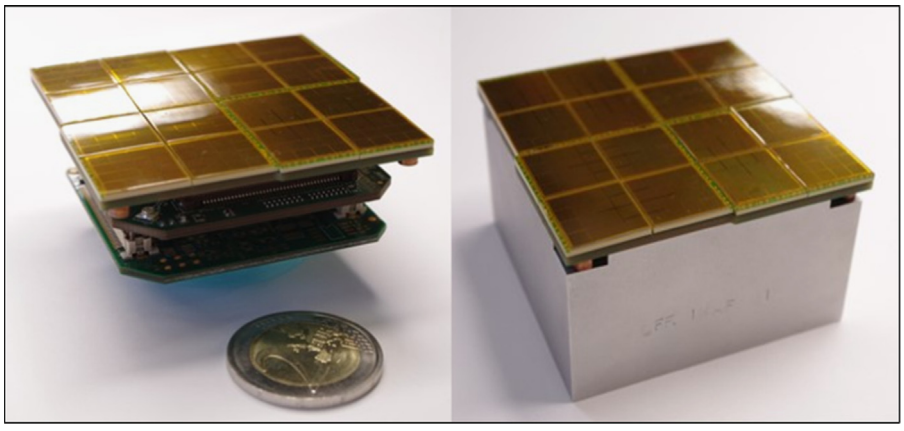

Fig. 5. PDM front-end PCBs accommodated in a dedicated PDM aluminum case.

ratio of 10, in agreement with the requirements for the maximum number of photoelectrons detected in one logical pixel. Each pre-amplifier is followed by a tunable slow-shaper and a track-and-hold circuit to catch the peak of the shaped signal. The sampled ampli tude of all signals can be read out by a pair of multiplexers (one for LG and one for HG) and subsequently converted by an external ADC. A separate chain is additionally implemented to generate a trigger signal, composed of a fast shaper followed by two discriminators with independent threshold settings.

One of the most important characteristics of this ASIC is that it provides 32 independent trigger output lines, one per pixel, allowing the generation of a global trigger signal based on the pattern of all

fired pixels in a very smart and efficient way from each PDM FPGA. Furthermore, each of the CITIROC channels is internally connected to an 8-bit Digital-to-Analog Converter (DAC) which finely adjust the SiPMs bias voltage, allowing gain stabilization.

In order to process the 64 PDM pixels, 2 CITIROC ASICs are connected in daisy chain, and 2 dual-channel 14 bit ADCs convert LG and HG sampled data values. Each ASIC is configured at the desired function by serially loading the specific configuration table in slow control mode.

A Xilinx Artix-7 FPGA governs and controls all operations inherent to the front-end PDMs, and communicates through dedicated bidirectional serial lines with the BEE, which has the role of concentrating, distributing, synchronizing and transmitting scientific data, ancillary data, housekeeping and control data from/to each PDM and the external system (workstation-console), in which quick-look, monitoring functions and data archiving are implemented.

The modular stacking of the PDM front-end PCBs and their accommodation in a dedicated aluminum case is depicted in Fig. 5. The PCBs are tied together in order to minimize space and optimize heat exchange between them.

4. Devices and methods

In this section, the experimental apparatus engaged for the detectors characterization is briefly discussed.

The main instruments involved in the electrical experimental set-up basically include a pulsed diode laser, a power supply and amplification unit (PSAU), produced by CAEN Electronics, and a two-channel digitizer. The PSAU is an electronic system embedding a power supply and a tunable amplification unit. It provides the cathode voltage for the SiPM detector in a range of 0–120 V with a 16 bit resolution, and features a variable amplification factor up to 50 dB. It integrates a feedback circuit to stabilize the operating voltage (and, in turn, the sensor gain) against thermal variations and a leading edge discriminator feeding an internal counter. In addition, the system can provide a digital output with a tunable width from 20 ns to 320 ns. All parameters can be programmed and monitored via a standard USB interface. An additional holder interface has been implemented for the SiPM electrical board to be connected to the PSAU, and a mechanical cooling adapter has also been realized, allowing to operate the SiPM from room temperatures down to 10 °C. The simplified block diagram of the supply/amplification system is illustrated in Fig. 6, where the core functional blocks are highlighted. The pulse generator used as light source is a pulsed diode laser driver unit, featuring controls for laser intensity and repetition frequency (8.0–0.5 MHz), and providing a synchronization output for triggering other connected devices. The laser head has a wavelength emission in the range of 408–409 nm, a maximum optical power of 0–250 mW, and a minimum pulse width of 44 ps, and is further equipped with an optical collimator. A mechanical adapter has been specifically realized to connect the laser head with the SiPM housing. The two-channel digitizer is sampled at 250 MS/s by a 12 bit ADC, and can be programmed and monitored via a USB interface.

The set-up exploited for SiPM gain measurements is sketched in Fig. 7. The pulsed diode laser allows to illuminate the SiPM detector with a light source of adjustable intensity and duration. A mechanical adapter connects the laser head to the SiPM detector housed in the PSAU. The SiPM device is biased and its output signal is amplified, digitalized, and PC-interfaced and controlled by specific applications allowing to acquire the digital signals, trace charge histograms, and save all of the processed information.

In addition, electrical measurements as a function of temperature are also carried out through the same apparatus set-ups as depicted in Fig. 7. To this purpose, a thermostatic camera has been realized to host the SiPM detector in adiabatic conditions, and a thermoelectric recirculating chiller has been exploited to cool the device and achieve the desired temperature.

The set-up exploited for SiPM optical measurements makes use of optical systems, such as light sources, precision filters, a monochromator and an integrating sphere, and partially based on particle counting equipment. The optical equipment used for detectors characterization is sketched in Fig. 8.

A xenon lamp is used as a radiation source; a wavelength selection system constituted by a set of band-pass filters and mirrors, and a Czerny–Turner monochromator are exploited to achieve the desired wavelength in the 130–1100 nm spectral range, with a FWHM smaller than 1 nm. A beam splitter is employed to direct the monochromatic radiation through an optical lens towards an integrating sphere, which hosts, in one port, a 1 cm^2 NIST-traced reference photodiode along with the SiPM sensor to be characterized.

The photon flux intensity coming into the integrating sphere can be regulated by means of neutral density filters or changing the aperture of the entrance or exit slits of the monochromator. Due to the small dimensions of the detectors to be characterized with respect to the optical beam, the integrating sphere is used to spatially integrate the radiant flux. Furthermore, appropriate mechanical structures are realized, in terms of both aperture and distance from the center of the sphere, to illuminate the SiPM detector and the NIST-traced photodiode with the same radiant flux. The reference photodiode allows to evaluate the number of photons per unit area, and then, after a proper rescaling, the number of photons impinging on the detectors under test.

The experimental set-up used for photon detection efficiency (PDE) measurements is sketched in Fig. 9.

Before executing the final PDE tests, the appropriate discriminator threshold must be selected to catch the SiPM pulses. For this purpose, the section of the PDE apparatus enclosed in the red-dashed box in Fig. 9 is exploited to trace the thermal noise rate plots. In particular, the SiPM thermal noise signal is amplified and fed into a discriminator module, generating a logic output pulse each time a dark pulse crosses a predefined voltage level, allowing to select the appropriate threshold to be used for the PDE measurements and evaluate the crosstalk contribution.

Once the optimal threshold is established, the discriminator digital output is connected to a TDC (as shown in the section delimited by the green-dashed line in Fig. 9). The software realized to control the TDC allows to acquire and save each recorded time tag. The data can be analyzed to reconstruct a histogram of the number of events as a function of the time interval between two adjacent pulses, and evaluate the presence of extra-charge noise.

Final PDE measurements involve the exploitation of the full apparatus in Fig. 9, where the SiPM detector and the reference photodiode are mounted together onto the integrating sphere to be illuminated with a monochromatic light. PDE tests are performed based on the measured SiPM count rate compared to the photocurrent signal from the NIST-calibrated photodiode. Tests are performed adjusting the photon flux level such that the reference diode is still sensitive and the SiPM detectors are safely in the single-photon regime with negligible pile-up. Moreover, the introduction of a calibrated neutral density filter in front of the SiPM allows to operate at sufficiently high current levels on the calibrated photodiode to avoid low signal measurements and hence achieve a reduction in the experimental error bars.

5. MPPC detectors characterization

In this section, electro-optical characterization of the basic 3×3 mm^2 single-pixel of the S11828-3344 MPPC detector is carried out and discussed.

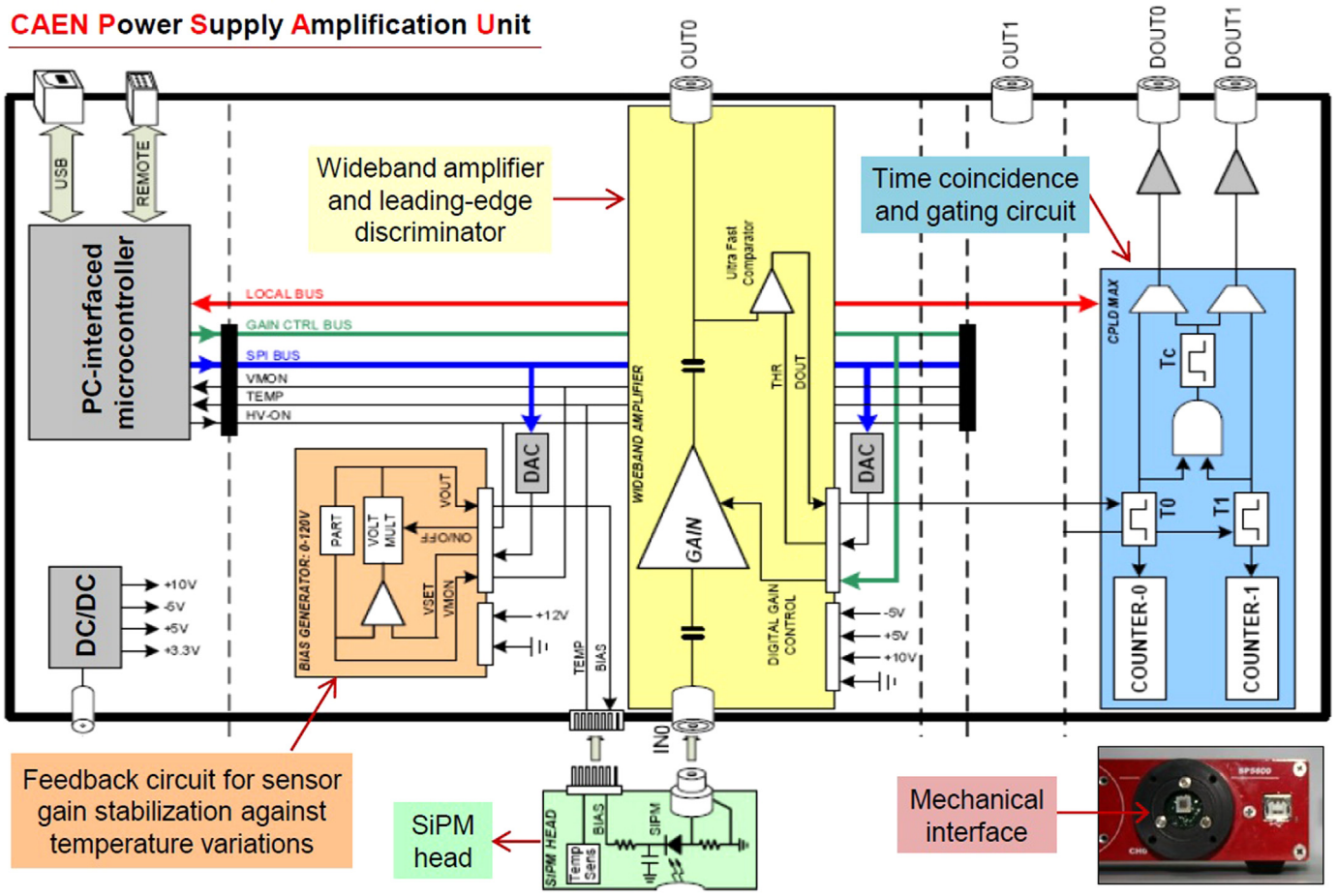

Fig. 6. Simplified schematization of the power-supply/amplification unit, developed by CAEN electronics.

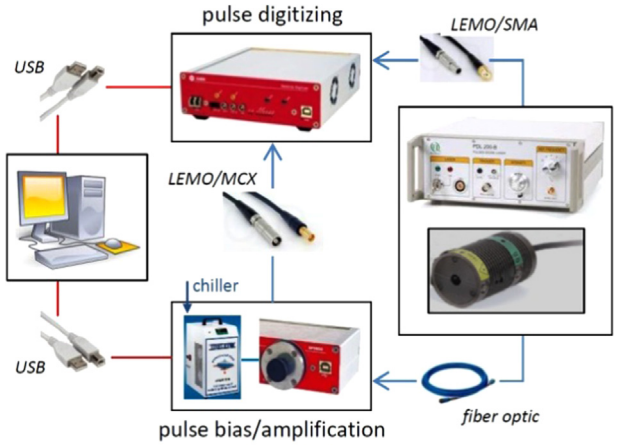

Fig. 7. Experimental apparatus used for SiPM gain measurements.

5.1. Gain measurements

The detector gain G is defined as the number of unit (electron) charges generated in response to a single-pixel photon absorption or thermally ignited avalanche. In Geiger-mode operation the multiplication factor of an avalanche discharge is expected to grow linearly with the operating voltage according to

$$G = \frac{Q_{TOT}}{q} = \frac{C_{pixel}(V_{OP} - V_{BD})}{q} \quad (1)$$

where Q_{TOT} is the total charge generated by a single avalanche discharge, C_{pixel} is the overall capacitance of the basic microcell, q is the elementary electron charge, V_{OP} is the operating voltage and V_{BD} is the detector breakdown potential. The term in round brackets in Eq. (1), better known as overvoltage or excess bias voltage, V_{OV}, is critical in defining the major performance parameters of SiPM detectors.

To evaluate the detector gain at a given temperature for a defined range of bias voltages, the integrated charge values from the multi-channel analyzer are filled into charge amplitude histograms and the average spacing between two adjacent curve peaks is computed (in terms of ADC channels). Consequently, by accounting for the constant ADC rate (charge/channel), and scaling by the amplifier gain factor, the SiPM gain is obtained for a given bias voltage.

To increase data statistics and improve precision, charge histograms are carried out upon illuminating the SiPM detector. In particular, for each performed acquisition, laser flux intensity and integration time windows are designed so as to achieve a large number of charge peaks with more than 10^4 occurrences.

Fig. 10 illustrates the charge pulse histograms of the MPPC device at 25 °C and for different operating conditions. Each observed peak corresponds to a specific number of fired pixels. Every pulse spectrum can be fit by a series of Gaussian distributions, with the μ parameter for each curve fit indicating the mean charge in the relevant peak and the σ parameter representing its width due to gain fluctuations and electronics noise [19].

The photoelectron peaks are visible, demonstrating a photoelectron resolution (maximum number of peaks that can be distinguished) of the MPPC device of at least 12 photoelectrons.

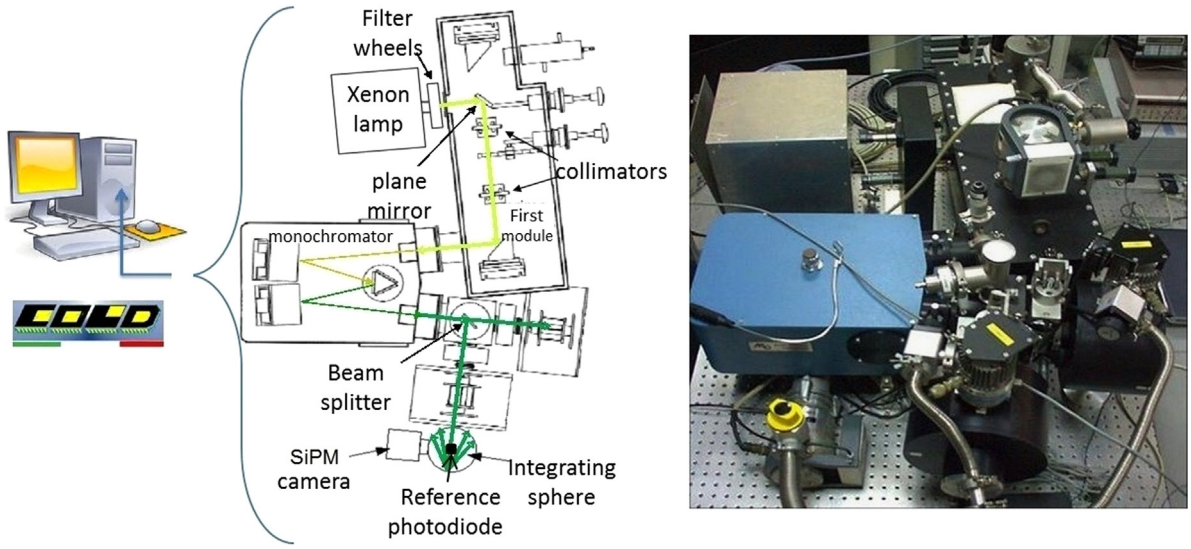

Fig. 8. Simplified diagram of the optical apparatus (on the left) and relevant instrumental equipment (on the right). The green line indicates the light path. (For interpretation of the references to color in this figure legend, the reader is referred to the web version of this article.)

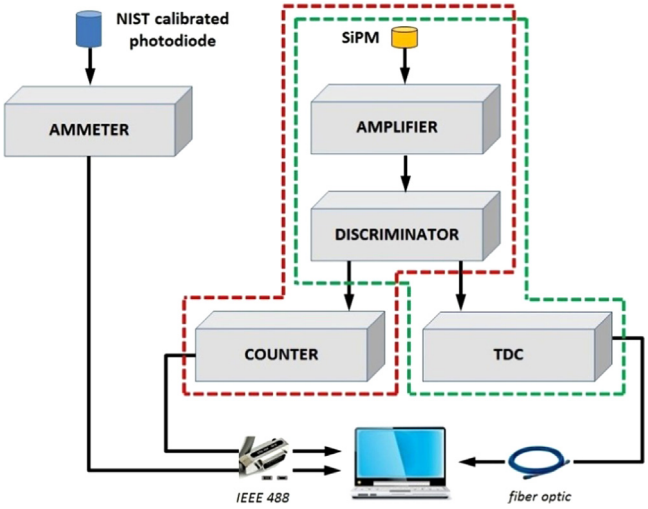

Fig. 9. Overview of the experimental apparatus set-up implemented for dark staircase (red-dashed box), extra-charge (green-dashed box) and photon detection efficiency (whole system) measurements. (For interpretation of the references to color in this figure legend, the reader is referred to the web version of this article.)

The average spacing between two consecutive charge peaks almost linearly increases with the bias conditions. All gain data points in a pre-defined range of operating voltages are collected in Fig. 11 for the same detector and equal working temperature. The extrapolation of the *x*-axis intercept of the linear fit in the gain plot as a function of the bias voltage provides a reasonable estimate of the breakdown voltage (70.5 V).

5.2. Dark and cross-talk measurements

The dark current is one of the crucial parameters affecting the performance of SiPM detectors. The noise figure for a Geiger-mode photosensor is identified with the dark count rate (DCR), defined as the number of avalanche current pulses produced by thermally generated carriers simulating the detection of single photons at a certain bias voltage.

A DCR scan plot of the MPPC device as a function of the discriminator threshold V_{TH} is reported in Fig. 12 at different temperature values. During thermal noise rate measurements the SiPM is kept in dark. Characteristic step curves are observed, and the count rates sharply drop (typically by one order of magnitude in frequency) when integer multiples of a 1 pe threshold are reached. For a threshold above the electronics noise and below the 1 pe amplitude, all thermally generated excitations are counted, so that the corresponding measure provides a fair estimation of the SiPM dark rate. Such kinds of plots are often referred to as staircase functions or, simply, stairs.

As derived by the plot, the SiPM DCR doubles approximately every 7 °C rise in temperature.

For all following measurements the optimal threshold level V_{TH}, also reported in Fig. 12, can be determined by the DCR measures at half-photon threshold, that is for a discriminator threshold corresponding to half the signal of the first photon pulse.

The experimental approach used for assessing the SiPM cross-talk probability relies on the analysis of DCR measurement results. For ideal detectors, the probability of two or more simultaneous thermal excitations should be marginal, so that only dark events corresponding to single photoelectrons should be observed. On the other side, in real SiPM sensors, spurious cross-talk induced avalanches can occur resulting in higher amplitude pulses. By comparing the measured event rates above 1 pe threshold with the total dark rate the cross-talk probability is estimated.

SiPM optical cross-talk is evaluated from the DCR data as the ratio between the first and the second event count rate. This approach is based on the assumption that the probability of triggering two uncorrelated avalanches within the same rise time is negligible.

Dark and cross-talk functional dependency on the operating voltage is also investigated. Cross-talk and DCR measurements results of the analyzed detector for different operating voltages are illustrated in Fig. 13 at $T=25$ °C, where the rising trends of both parameters are observed.

As inspected from the above plots, in the analyzed range of operating voltages the SiPM DCR and cross-talk values keep lower than 700 kHz and 22%, respectively.

The final operating voltage for the ASTRI SST-2M camera will be selected based on the optimal trade-off between DCR and cross-talk results, on the one side, and the relevant PDE measurements, on the other side, obtained at the final working temperature.

5.3. Extra charge measurements

Photon counting resolution of SiPM devices may be affected by correlated extra-charge effects, resulting in additional pulse counts

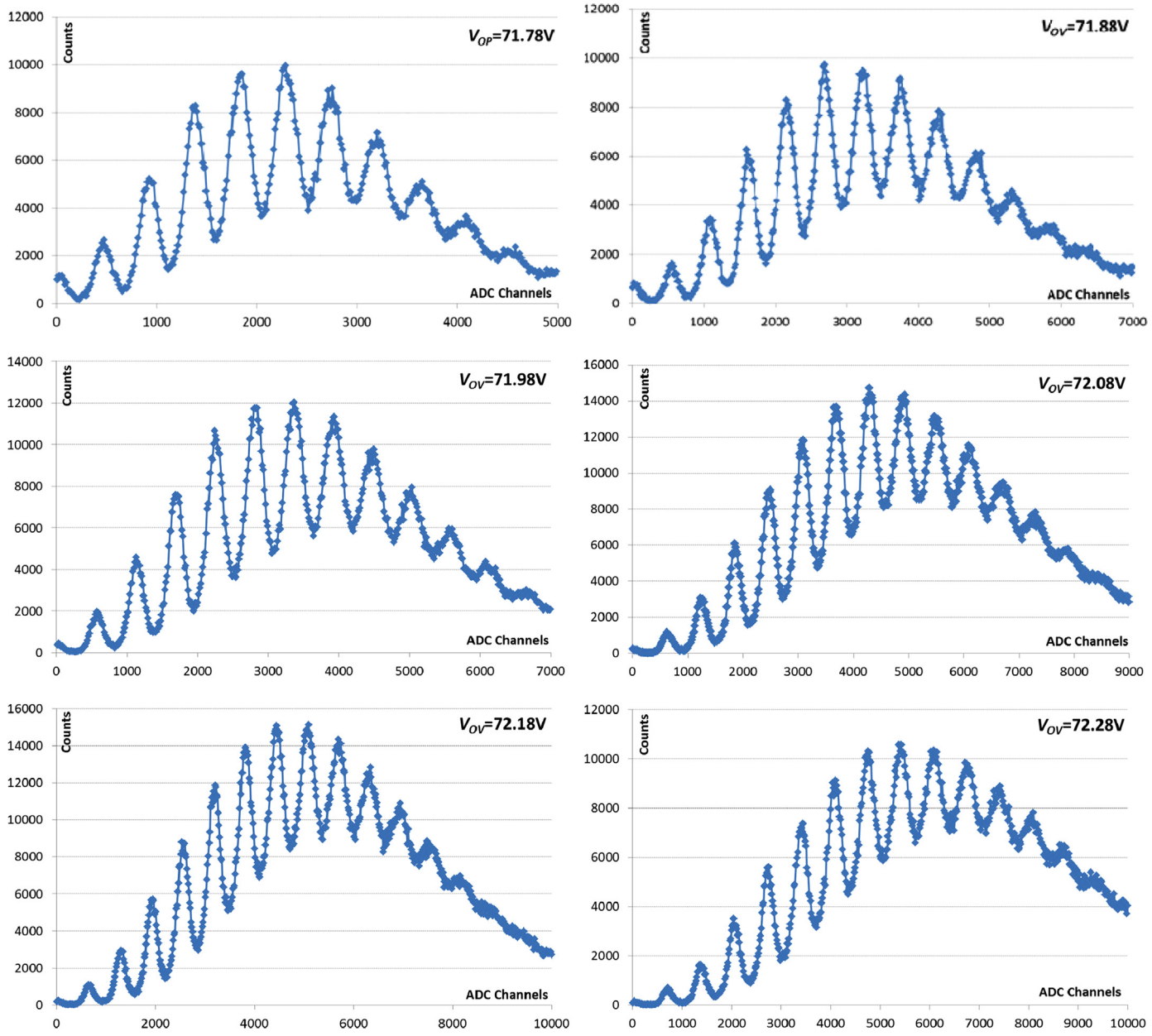

Fig. 10. Charge–amplitude histograms of the MPPC device for different bias conditions (T=25 °C).

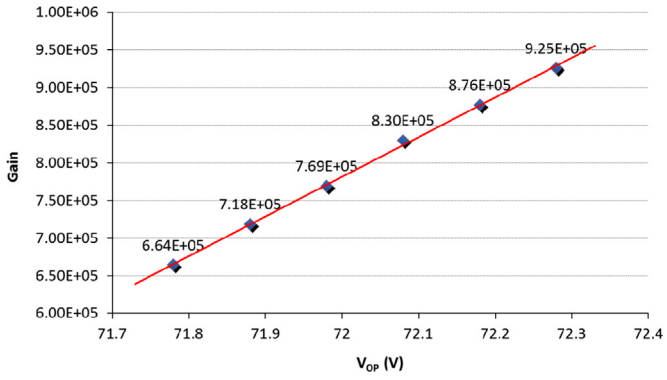

Fig. 11. Gain measurements of the MPPC device as a function of the bias voltage. The linear fit allows to extrapolate the breakdown potential.

which are delayed with respect to the original avalanche discharges. Such excess noise effects may include afterpulsing and delayed or indirect optical cross-talk. Such extra-charge effects are hardly distinguished and result in an over-estimation of the SiPM detection efficiency.

To evaluate the amount and contribution of extra noise to the real signals, frequency histograms of the time intervals between two consecutive pulse signals are carried out for the detector under test; Fig. 14 illustrates these distributions (blue dots). The measured values in the 0–3000 ns region are fitted with a double exponential function (violet line), representing both dark (red line) and extra-charge (green line) contributions, whose expression (approximation of Eq. (6) in [7]) is

$$f(t) = A_{dark} e^{-t/\tau_{dark}} + A_{ex} e^{-t/\tau_{ex}} \quad (2)$$

where A_{dark} and A_{ex} are respectively the weights of the pure dark counts and extra-charge noise, while τ_{dark} and τ_{ex} are the time constants associated to the foregoing processes.

The fit functions obtained from the experimental data can be used to provide an immediate assessment of the DCR (represented by the reciprocal of parameter τ_{dark}), which can be checked against the relevant values measured through a direct counting. A dark

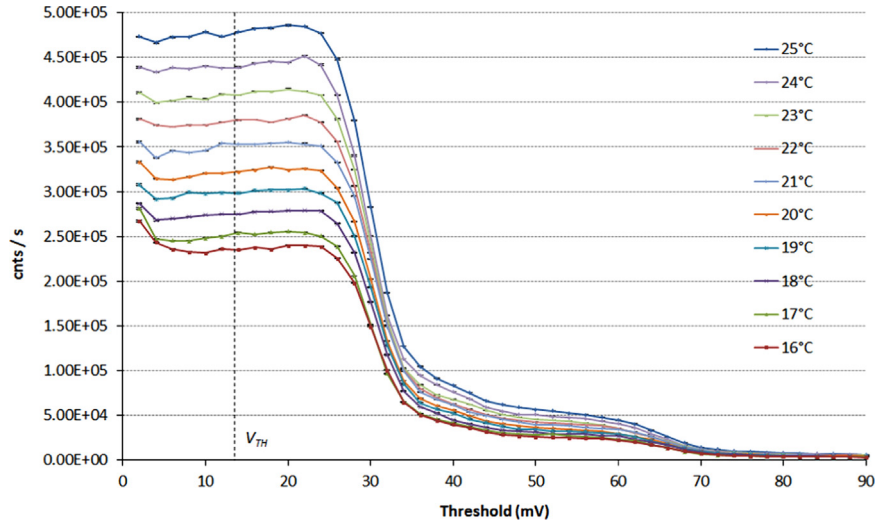

Fig. 12. Dark staircase functions of the MPPC device for a fixed operating voltage (71.98 V) and different temperature values.

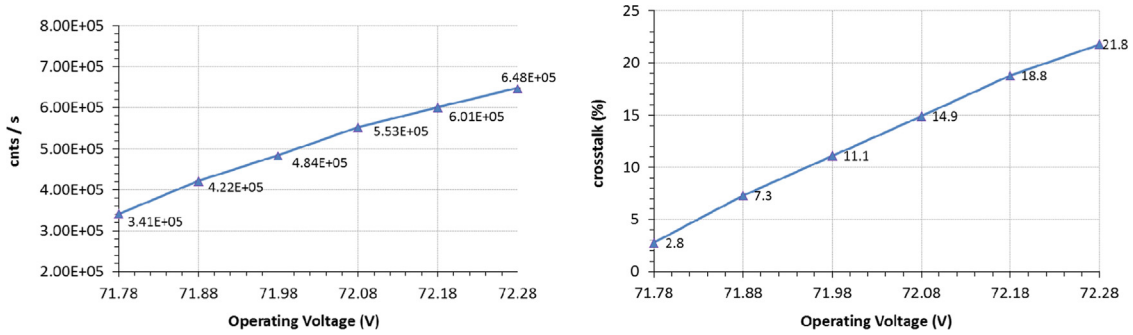

Fig. 13. Dark stairs (on the left) and optical cross-talk (on the right) measurement results of the MPPC device at $T=25$ °C as a function of the operating voltage.

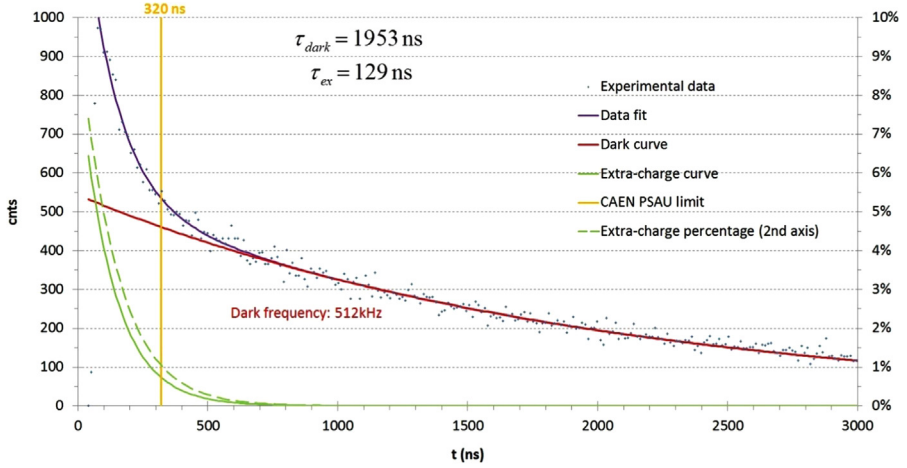

Fig. 14. Histograms of the time interval between two consecutive pulses and relevant fit curve for a fixed operating voltage (71.98 V) at 25 °C. The extra-charge contribution is represented by the continuous green line, and its percentage over the total number of events is shown by the green-dashed line. The low cut-off value of the experimental data is 75 ns. (For interpretation of the references to color in this figure legend, the reader is referred to the web version of this article.)

frequency value of 512 kHz is extracted by Fig. 14 (red label), and the close correspondence between this value and the 0.5 pe DCR data in Fig. 12 at the same operating conditions gives confidence on the correctness of the measurement results.

Referring to the distributions in Fig. 14, the green-dashed line represents the percentage of the extra-charge noise over the total number of events, from which it can be noted that extra-charge effects are observable as far as about 0.85 μs. The vertical yellow line represents the maximum applicable hold-off time (320 ns) resulting from the highest digital output width from the PSAU, at which the residual extra noise percentage is less than 1%.

Therefore, to reduce as much as possible the effects of extra-charge for PDE measurements, a controlled hold-off time is introduced by the measurement system for each detected pulse, and a statistical dead time correction is applied to account for the lost pulse signal. The dead time correction applied is based on the

assumption that the arrival time of the incident photons is expected to follow a statistical Poissonian distribution, and is expressed by the following relationship [21]:

$$S_c = \frac{S_0}{1 - t_{hold} S_0} \tag{3}$$

where S_0 is the number of counts per second, t_{hold} is the applied hold-off time, and S_c is the corrected count rate.

5.4. Photon detection efficiency measurements

Absolute PDE measurements are performed based on the photon counting method, by which the number of pulses per unit time in monochromatic light conditions are compared to the light level recorded by a reference NIST photodetector at the same time and for several wavelengths.

The effective number (subtracted for dark counts) of SiPM pulse counts per second detected by the counter module for a 0.5 pe discriminator threshold, Φ_{det}, is evaluated over a large wavelengths spectrum and for different bias voltages to obtain the corresponding PDE measurements, yielding

$$PDE = \frac{\Phi_{det}}{\Phi_{inc}} \tag{4}$$

where Φ_{inc} is the effective incident photon rate on the MPPC detector, which, under uniform illumination conditions, is derived from the photon flux rate on the calibrated photodiode, Φ_{PH}, according to

$$\Phi_{inc} = \Phi_{PH} \frac{A_{MPPC}}{A_{PH}} T_{filter} \tag{5}$$

where A_{MPPC} and A_{PH} are the known MPPC and reference photodiode sensitive areas, respectively, and T_f the transmittance of the neutral density filter exploited for attenuating the incident light flux on the detector.

The photon flux rate on the calibrated photodiode can be evaluated starting from the measured current produced as a result of the effective number of incident photons per unit time, and is calculated as

$$\Phi_{PH} = \frac{1}{QE} \frac{I_{mPH} - I_{dPH}}{q} \tag{6}$$

where I_{mPH} and I_{dPH} are respectively the reference photodiode currents measured under illumination and dark conditions, and QE_{PH} is its NIST traced quantum efficiency at the same operating wavelength.

Fig. 15 illustrates the PDE measurements of the MPPC detector in the 350–950 nm range of wavelengths and for different operating conditions. A 320 ns hold-off time is applied for all curves to reduce as much as possible any extra-charge effects. Dark noise contributions are removed.

It is worth remarking that the adopted photon counting technique to determine the detector PDE does not account for cross-talk, as a unique 0.5 pe threshold is applied to all pulses.

PDE measurement results of the analyzed detector as a function of dark counts and cross-talk at two different wavelengths are shown in Fig. 16. Each single data curve in the plot indicates the DRC and cross-talk functional dependencies on the SiPM bias condition, since higher x-axis points result from increased operating voltages.

The above plot can be usefully exploited for comparing the photon detecting capabilities of the characterized SiPM within the maximum allowed values of the most important noise sources (cross-talk and dark) dictated by the specific application requirements. On the other hand, such measurement results can be useful in evaluating the best operating condition for the SiPM as a result of an optimal trade-off between PDE and cross-talk, from one side, and PDE and DCR, from the other side; in fact, higher PDE values are obtained at greater bias voltages at the cost of increased cross-talk and DCR.

6. General discussion

The challenging decision of using MPPC sensors for the ASTRI SST-2M prototype camera is the result of many technical and scientific considerations. ASTRI SST-2M optics design (two mirrors)

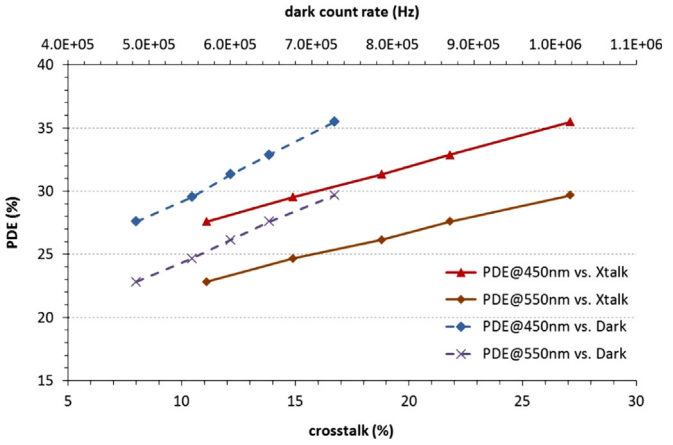

Fig. 16. PDE versus DCR (primary axis) and cross-talk (secondary axis) for the MPPC detector and for two different wavelengths and T=25 °C.

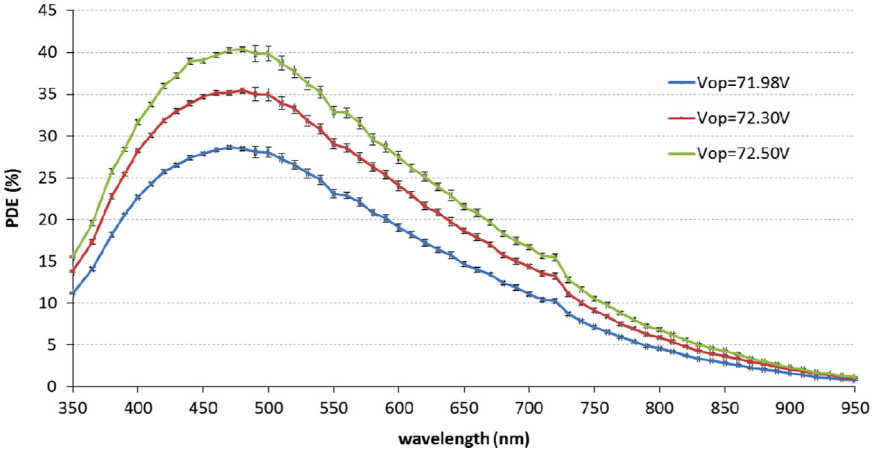

Fig. 15. PDE measurements as a function of wavelength of the MPPC detector for different operating voltages and T=25 °C.

involves a reduction in the size of the focal surface with respect to the usual optics design (Davis–Cotton mirror). This in turn implies a pixel size in the order of few millimeters to cover the required field of view with a pixel angular size of $\sim 0.2^{\circ}$, as dictated by CTA for the small-size telescope types. Due to the resulting camera high pixelization, only Multi-Anode Photo-Multiplier (MAPMT) or SiPM detectors comply with this requirement in term of pixel size.

Silicon sensors are presently the novel kind of solid-state devices that will be hopefully supported and further developed by the light-sensor manufacturing companies in the coming years, while this could not be the case for MAMPTs. On the other hand, silicon devices offer a number of attractive advantages, such as small packaging, weight and power consuming, and can survive to intense light exposure compared to MAMPTs. Another characteristic that differentiates silicon devices from MAPMTs is their high performance in photon counting contexts. From a technical point of view, SiPM sensors allow to design a compact, low power consuming camera offering similar performance (if not superior) with respect to MAPMTs.

The aim of the ASTRI SST-2M prototype is to verify the performance of the entire design in the field. From scientific point of view, extension of the duty cycle of telescope operation is expected, due to the possibility to operate the telescope even in presence of the Moon. In addition, by using SiPM sensors, a more accurate energy measurement is foreseen.

The camera prototype aims to demonstrate through performance studies the feasibility of using silicon sensors for Cherenkov telescopes. Although this particular MPPC detector does not offer the same performance as current devices (new sensors with superb features are today available by manufacturing companies such as Hamamatsu, Excelitas, FBK, etc.), based on measurement results carried out on the characterized detector it is expected that its performance can be sufficiently appropriate to draw conclusions on the entire processing system.

The final operating voltage for the MPPCs will be set according to the stabilized temperature of the camera, which is foreseen in the range of 15–20 °C. The front-end ASICs allow to adjust pixel-by-pixel the MPPCs gain in a wide range of temperatures with a fine resolution of ~ 20 mV, corresponding to $\sim 1/3\,\mathrm{C}^{\circ}$ step. This feature, together with the continuous monitoring of the MPPC temperatures during camera operation, allows to correct any possible temperature gradient on the focal plane surface by increasing or decreasing the pixel bias voltage with respect to a reference operating voltage, which will be decided after the calibration test phase on the integrated camera.

7. Conclusions

A systematic and detailed characterization methodology for the MPPC detectors of the ASTRI SST-2M camera is discussed, with the aim of providing accurate measurements of the most important electro-optical parameters and qualifying the overall device performance. Experimental results of a large set of measurements on the basic MPPC device are performed, in order to provide a reliable qualification of the detector performance and evaluate its compliance with the telescope focal plane requirements. In particular, breakdown voltage, internal gain, dark count rate, cross-talk and extra-charge probability, and absolute photon detection efficiency measurements are performed on the basic sensor device unit as a function of the detector operating conditions.

This kind of detectors are a preliminary version for the ASTRI SST-2M camera; however, characterization results confirm that their performance will allow sufficiently accurate energy measurements on the field. Testing activities on new recently developed detectors are ongoing, according to the technological development of the SiPM manufacturers. As a matter of fact, both the mechanical structure and the front-end electronics of the telescope camera will remain the same for the upcoming CTA-SST mini-array project, and thus these detectors are also expected to provide useful information on the global electronics performance.

Acknowledgments

This work was partially supported by the ASTRI “Flagship Project”, financed by Ministero dell'Istruzione, dell'Università e della Ricerca the Italian Ministry of Education, University, and Research (MIUR) and led by the Italian National Institute for Astrophysics (INAF).

We gratefully acknowledge support from the agencies and organizations listed under funding agencies at this website: http://www.cta-observatory.org/.

References

[1] M. Actis, et al., Experimental Astronomy 32 (3) (2011) 193.
[2] R. Canestrari, et al., on behalf of the ASTRI collaboration, Proceedings of the 32nd International Cosmic Ray Conference, vol. 9, 2011, pp. 115–118.
[3] G. Bonanno, et al., Nuclear Instruments and Methods in Physics Research A 610 (1) (2009) 93.
[4] J. Fleury, et al., Journal of Instrumentation 9 (1) (2014), C01049.
[5] S. Callier, C. de La Taille, G. Martin-Chassarda, L. Raux, EASIROC, an easy and versatile readout device for SiPM, in: Proceedings of the TIPP, 2001.
[6] D. Marano, et al., IEEE Sensors Journal 14 (8) (2014) 2749.
[7] A. Vacherect, et al., Nuclear Instruments and Methods in Physics Research A 656 (1) (2011) 69.
[8] C. Piemonte, et al., IEEE Transactions on Nuclear Science NS54 (1) (2007) 236.
[9] E. Sciacca, et al., IEEE Transactions on Electron Devices ED50 (4) (2003) 918.
[10] P. Eckert, et al., Nuclear Instruments and Methods in Physics Research A 620 (1) (2010) 217.
[11] M. Petasecca, et al., IEEE Transactions on Nuclear Science NS55 (3) (2008) 1686.
[12] S.K. Yang, et al., Optics Express 22 (1) (2014) 716.
[13] S. Billotta, et al., Journal of Modern Optics 52 (2–3) (2009) 273.
[14] M. Belluso, et al., Characterization of SPAD arrays: first results, in: J.E. Beletic, J.W. Beletic, P. Amico (Eds.), Scientific Detectors for Astronomy, vol. LXIV, Berlin: Springer, Dordrecht, 2006, p. 469 (1-4020-4329-5).
[15] D. Marano, et al., Nuclear Instruments and Methods in Physics Research A 726 (2013) 1.
[16] D. Marano, et al., IEEE Transactions on Nuclear Science NS61 (1) (2014) 23.
[17] D. Impiombato, et al., Evaluation of the Optical Cross Talk Level in the SiPMs Adpted in ASTRI SST-2M Cherenkov Camera Using EASIROC Front-end Electronics, arXiv:1312.0381, 2013.
[18] G. Bonanno, et al., IEEE Sensors Journal 14 (10) (2014) 3557.
[19] G. Bonanno, et al., IEEE Sensors Journal 14 (10) (2014) 3567.
[20] V. DeCaprio, et al., The ASTRI SST-2M prototype: camera design, in: Proceedings of the SPIE, 2013.
[21] V. O'Connor, D. Phillips, Time-Correlated Single Photon Counting, Academic Press, London, 1984.
[22] O. Soto, et al., Nuclear Instruments and Methods in Physics Research A 732 (2013) 431.
[23] V. Boccone, et al., Characterization of new hexagonal large-area geiger avalanche photodiodes, in Proceedings of the IEEE ANIMMA, 2013, pp. 1–6.